



Self-training via Metric Learning for Source-Free Domain Adaptation of Semantic Segmentation

Ibrahim Batuhan Akkaya^{a,**}, Ugur Halici^a

^aMiddle East Technical University, Ankara 06800, Turkey

ABSTRACT

Unsupervised source-free domain adaptation methods aim to train a model for the target domain utilizing a pretrained source-domain model and unlabeled target-domain data, particularly when accessibility to source data is restricted due to intellectual property or privacy concerns. Traditional methods usually use self-training with pseudo-labeling, which is often subjected to thresholding based on prediction confidence. However, such thresholding limits the effectiveness of self-training due to insufficient supervision. This issue becomes more severe in a source-free setting, where supervision comes solely from the predictions of the pre-trained source model. In this study, we propose a novel approach by incorporating a mean-teacher model, wherein the student network is trained using all predictions from the teacher network. Instead of employing thresholding on predictions, we introduce a method to weight the gradients calculated from pseudo-labels based on the reliability of the teacher's predictions. To assess reliability, we introduce a novel approach using proxy-based metric learning. Our method is evaluated in synthetic-to-real and cross-city scenarios, demonstrating superior performance compared to existing state-of-the-art methods.

© 2024 Elsevier Ltd. All rights reserved.

1. Introduction

Recent advancements in deep learning have led to notable improvement in the field of computer vision. Deep learning networks trained in a supervised manner demonstrate high performance, even in challenging tasks that require dense prediction, such as semantic segmentation (Chen et al., 2017b,a; Wang et al., 2020a; Zhong et al., 2020; Xu et al., 2023; Fan et al., 2021). However, the preparation of large datasets with dense labeling is a laborious and expensive process (Cordts et al., 2016). One approach to mitigate the workforce requirements involves the use of publicly available real datasets (Everingham et al., 2010; Cordts et al., 2016; Chen et al., 2017c) or synthetic

datasets (Richter et al., 2016; Ros et al., 2016). However, it is important to note that deep learning approaches typically assume the Identically and Independently Distributed (IID) distribution of training and testing sets. Given the distinct marginal distributions between the source and target domains, the trained model experiences performance degradation when evaluated on the target data — a phenomenon known as the domain gap.

Various domain adaptation methods have been introduced to address the challenge of domain gap (Sankaranarayanan et al., 2018; Du et al., 2019; Tsai et al., 2018; Araslanov and Roth, 2021; Pan et al., 2020; Xu et al., 2021; Zhou et al., 2020; Hoyer et al., 2023). These approaches leverage both labeled data from a source domain and unlabeled data from a target domain during model training. However, in certain applications such as medical imaging or autonomous driving, accessing la-

**Corresponding author:

e-mail: bthakkaya@gmail.com (Ibrahim Batuhan Akkaya)

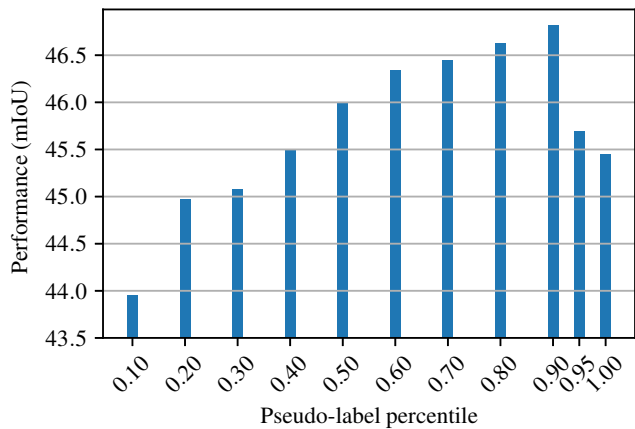


Fig. 1. Segmentation performance of the self-training when different percentile of the predictions are used as pseudo-labels

beled source domain data may be restricted due to intellectual property (IP) or privacy concerns. To overcome this limitation, an alternative solution involves utilizing a model trained on the source domain instead of the actual data. This approach, known as source-free domain adaptation, aims to reduce the domain gap by employing a source model alongside unlabeled target domain data.

Self-training is a widely utilized technique in both classical domain adaptation and source-free domain adaptation (Liu et al., 2021a; Herath et al., 2023; Karim et al., 2023). This training strategy involves adapting the model using pseudo-labels generated by the model itself. Many approaches incorporate prediction filtering mechanisms to determine these pseudo-labels (Zou et al., 2018, 2019; Mei et al., 2020; Li et al., 2019). In the context of source-free domain adaptation, where supervision relies exclusively on the target dataset due to the absence of a source dataset, harnessing predictions from target images becomes paramount during training. Thresholding the predictions in this scenario leads to a degradation of supervision. Conversely, utilizing all predictions is suboptimal, as erroneous predictions can misguide the training process, resulting in performance deterioration, as illustrated in Figure 1. Consequently, instead of employing thresholding, our approach seeks to utilize all predictions by scaling the guidance based on the reliability of each prediction.

Assessing the reliability of predictions within the target domain presents a formidable challenge, as neural networks often exhibit overconfident false predictions when encountering data significantly deviating from learned training set patterns, such as out-of-distribution images (Hein et al., 2019). In the context of domain adaptation, where target dataset images are inherently out-of-distribution for a model trained on the source domain, establishing a domain-specific and reliable metric becomes imperative. Addressing this challenge, we propose a novel Self-Training via Metric learning (STvM) reliability measure tailored to the target domain. Our method uses pixel-level proxy-based metric learning to train a network that predicts distance metrics for each pixel in target domain images. The goal is to keep pixels from the same class close together, while keeping them far from pixels of other classes. By using proxy-based metric learning, we simultaneously train a feature vector for each class. These vectors act as class prototypes in the target domain. We then compute the reliability measure by evaluating the distance between the pixel feature and the proxy feature of the predicted class. This methodology greatly improves the model’s ability to assess reliability in the target domain. This is especially important when dealing with out-of-distribution images, a common situation given that images from the target domain are considered out-of-domain for a model trained in the source domain. Furthermore, we leverage the reliability metric to sample patches from the target domain, allowing us to adapt mixing augmentation effectively in the absence of labeled data.

In summary, our contributions are as follows:

- We introduce a novel reliability metric, learned directly in the target domain through a proxy-based metric learning approach.
- Unlike conventional methods that filter predictions for pseudo-labels, we employ all predictions in the self-training process and adjust the gradients based on the reliability metric.
- We devise an effective way to adapt mixing augmentation, dubbed as a metric-based online ClassMix, in the absence

of labeled data by leveraging the reliability metric to sample patches from the target domain.

- Our STvM (Self-Training via Metric-learning) approach demonstrates superior performance compared to state-of-the-art methods across GTA5-to-CityScapes, SYNTHIA-to-CityScapes, and NTHU datasets.

2. Related works

Domain adaptation. Domain adaptation is a widely studied topic, especially for image classification (Wang and Deng, 2018) and semantic segmentation (Toldo et al., 2020). Adversarial learning (Chang et al., 2019; Hong et al., 2018; Tsai et al., 2018; Chen et al., 2019b,c; Choi et al., 2019; Li et al., 2019) and self-training (Chen et al., 2019a; Iqbal and Ali, 2020; Mei et al., 2020; Pan et al., 2020; Zhang et al., 2019; Zheng and Yang, 2021; Zou et al., 2019, 2018) approaches are commonly utilized in semantic segmentation. Adversarial methods, inspired by the GAN framework (Goodfellow et al., 2014), align the feature space of the source and target. Unlike the GAN framework, these methods distinguish between source and target domains rather than real and fake samples. Adversarial learning is applied in image and feature levels. Some methods exploit the adversarial approach to the low-dimensional output space to facilitate adversarial learning. Self-training methods utilize confident predictions as pseudo-labels. These are obtained by filtering out noisy samples or applying constraints, and then used for supervised training.

Source-free domain adaptation. Source-free domain adaptation applies domain adaptation using only the trained source model instead of the source data as well as unlabeled target data, where the source data cannot be freely shared due to Intellectual Property of privacy concerns. The task is introduced by two works (Fleuret et al., 2021; Liu et al., 2021b) concurrently. URMA (Fleuret et al., 2021) reduces the uncertainty of predictions in the presence of feature noise. This is accomplished by using multiple decoders and incorporating feature noise through dropout. The model’s resistance to noise is pre-

served by an uncertainty loss, determined by the squared difference between the decoder outputs. The training stability is improved with entropy minimization and self-training with threshold-based pseudo-labeling. SFDA (Liu et al., 2021b) introduces a data-free knowledge distillation approach. It generates source domain synthetic images that preserve semantic information using batch-norm statistics of the model and dual-attention mechanism. They also use a self-supervision module to improve performance. HCL (Huang et al., 2021) proposed Historical Contrastive Learning (HCL), comprising Historical Contrastive Instance Discrimination (HCID) and Historical Contrastive Category Discrimination (HCCD). HCID contrasts embeddings of target samples from current and historical models, while HCCD employs pseudo-labels for learning category-discriminative representations. LD (You et al., 2021) highlights that self-training methods often face the ‘winner-takes-all’ issue, where majority classes dominate, leading to segmentation networks failing to classify minority classes. To remedy this, they propose a two-component framework: positive and negative learning. Positive learning selects class-balanced pseudo-labeled pixels using an intra-class threshold, while negative learning identifies the category to which each pixel does not belong through complementary label selection. DA+AC (Yang et al., 2022) presents a framework to stabilize SFDA for semantic segmentation. Initially, in the distribution transfer phase, it aligns source model features with target data statistics. Then, in the self-training stage, it employs adaptive thresholding to select per-class pseudo labels for self-supervision. GtA (Kundu et al., 2021) categorized the SF-UDA methods as a vendor and client-side strategies, where vendor-side strategies focus on the improving source model for better adaptation. They focus on improving the vendor side performance and propose multiple augmentation techniques to train different source models using the leave-one-out technique on the vendor side.

Considering that it may not be possible to train the model on the vendor-side in source-free scenario, we propose a client-side source free domain adaptation method like SFDA and

URMA, in which the source model is used as-is.

Metric learning. Deep metric learning (DML) is an approach to establish a distance metric between data to measure similarity. It learns an embedding space where similar examples are close to each other, and different examples are far away. It is a widely studied topic in computer vision that has various applications such as image retrieval (Movshovitz-Attias et al., 2017), clustering (Hershey et al., 2016), person re-identification (Cheng et al., 2016) and face recognition (Schroff et al., 2015). In the unsupervised domain adaptation literature, metric learning is mostly utilized in the image classification task. The features of the semantically similar samples from both source and target domain are aligned to mitigate the domain gap (Huang et al., 2015; Laradji and Babanezhad, 2020; Pinheiro, 2018; Yu et al., 2018). Commonly, the similarity metric between images or patches is trained in deep metric learning. With a different perspective, Chen et al. (Chen et al., 2018) utilize pixel-wise deep metric learning for interactive object segmentation, where they model the task as an image retrieval problem. DML approaches are categorized into two classes based on the loss functions, namely pair-based and proxy-based methods. While pair-based loss functions (Wang et al., 2019a,b; Oh Song et al., 2016; Sohn, 2016) exploit the data-to-data relations, the proxy-based loss functions (Movshovitz-Attias et al., 2017; Teh et al., 2020; Qian et al., 2019; Aziere and Todorovic, 2019) exploit data-to-proxy relations. Generally, the number of proxies is substantially smaller than training data. Therefore, proxy-based methods converge faster, and the training complexity is smaller than pair-based methods. They are also more robust to label noise and outliers (Kim et al., 2020).

In STvM, we propose a proxy-based pixel-wise metric learning to estimate pseudo-label reliability, trained by limited and noisy pseudo-labels.

Mixing. Mixing is an augmentation technique that combines pixels of two training images to create highly perturbed samples. It has been utilized in classification (Berthelot et al., 2019; Yun et al., 2019; Hongyi Zhang and Lopez-Paz, 2018) and semantic segmentation (French et al., 2020; Olsson et al.,

2021). Especially in semi-supervised learning of semantic segmentation, mixing methods, such as CutMix (Yun et al., 2019) and ClassMix (Olsson et al., 2021), achieved promising results. While the former cut rectangular regions from one image and paste them onto another, the latter use a binary mask belonging to some classes to cut. DACS (Tranheden et al., 2021) adapts ClassMix (Olsson et al., 2021) for domain adaptation by mixing across domains.

In source-free domain adaptation, access to the source domain dataset is not available. This makes it impossible to combine target images with source patches. Additionally, the absence of labels in the target domain dataset presents a challenge when trying to use ClassMix. In order to utilize mixing, we propose an metric based online ClassMix method where patches are sampled based on our reliability metric.

3. Proposed method

In this section, we present our self-training via metric learning (STvM) approach for the unsupervised source-free domain adaptation problem in the context of semantic segmentation. The source-free domain adaptation setting is composed of the following components. Let \mathcal{D}_S is a labeled source dataset composed of source domain images x_S and corresponding pixel-wise labels y_S , $\mathcal{D}_S = \{(x_S^i, y_S^i)\}_{i=1}^{N_S}$ where N_S is the number of samples in \mathcal{D}_S . It is assumed that the source model is trained with \mathcal{D}_S in a supervised manner so that it performs well in the source domain. Let \mathcal{D}_T is an unlabeled target dataset composed of target domain images, $\mathcal{D}_T = \{(x_T^i)\}_{i=1}^{N_T}$ where N_T is the number of samples in \mathcal{D}_T . The source-free domain adaptation technique involves training a model using a pretrained model from the source domain and an unlabeled dataset from the target domain \mathcal{D}_T . Our approach leverages the mean teacher model, which comprises two segmentation networks: the teacher network \mathcal{T} and the student network \mathcal{S} . We aim to incorporate source domain knowledge during the initial training phase and gradually adapt to the target domain. To achieve this, we initialize both models with the source domain-trained model. The student network’s parameters are updated

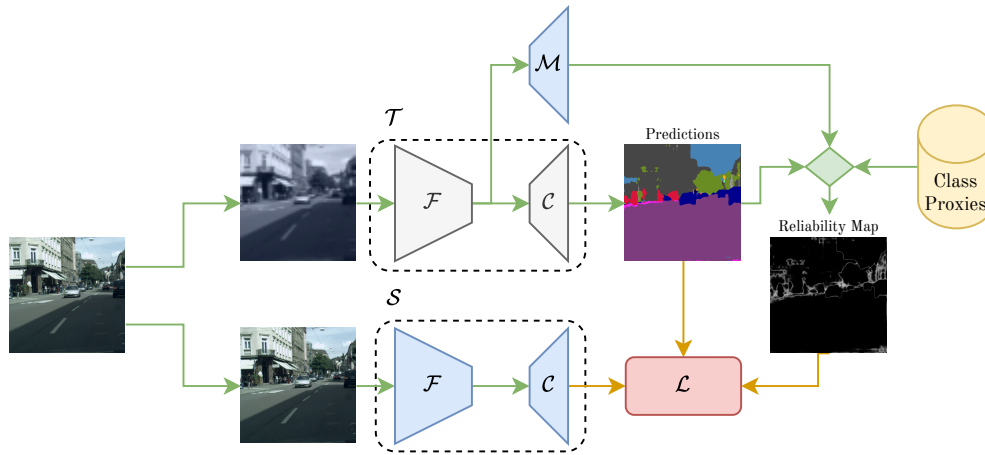


Fig. 2. STvM comprises three networks, namely teacher, student, and metric network, represented as \mathcal{T} , \mathcal{S} , and \mathcal{M} , respectively. The teacher and the student network use the same segmentation network architecture. Each segmentation network is composed of feature extractor \mathcal{F} and classifier \mathcal{C} . The metric network has the same architecture as \mathcal{C} , trained to learn metric feature space. Inspired by the mean-teacher approach, the student network is trained with a backpropagation algorithm. On the other hand, the parameters of the teacher model are updated with the moving average of the parameters of the student model. The metric network \mathcal{M} and class proxies are also trained with a backpropagation algorithm.

using gradient descent on the target dataset \mathcal{D}_T through a self-training approach. Meanwhile, the teacher network’s parameters are updated by exponentially averaging the student network’s parameters throughout the training process, facilitating a smooth transition from the source to the target domain.

3.1. Framework overview

The proposed method is illustrated in the Figure 2. We utilize the mean-teacher approach to train a segmentation model. There are two data paths in STvM: One belongs to the teacher and metric networks, and the other belongs to the student.

The teacher data path is responsible for training the metric network, generating the pseudo-labels and the reliability map. An image belonging to the target dataset is fed to the teacher network. The predictions of the teacher model are used as pseudo-labels. In addition to that, the features generated by the feature extractor of the teacher network are fed to the metric network to form metric features for each pixel of the input image. Class proxy features, trained in conjunction with the metric network, are vectors that represent the class distribution in the metric space. The distance between the proxy feature of the predicted class and the feature generated by the metric network is utilized as a measure of class similarity. This class similarity is subsequently transformed into a reliability score using the

reverse sigmoid function. The metric network is trained with a proxy-based metric learning approach using the highly confident predictions of the teacher network.

The student data path is responsible for the training of the student network using pseudo-labels and reliability scores. Firstly, A photometric augmentation is applied to the input image, then Metric-based Online ClassMix (MOCM) augmentation is applied to the input image, the pseudo-labels, and the reliability map. The patches that are used in MOCM are stored to the patch buffer in training time based on the metric similarity. The online patch update approach enables end-to-end training of the student model. The student model is trained with a pixel-wise cross-entropy loss function. However, the pixel-wise loss is multiplied with a reliability score to scale gradients which suppress erroneous pseudo-labels and allow under-confident accurate predictions to contribute to training.

3.2. Mean teacher with noisy student

The mean teacher method constitutes two networks called the teacher and the student networks (Tarvainen and Valpola, 2017). The parameters of the teacher network are updated by moving average of the student network parameters where the student network is updated with backpropagation. The mean

teacher approach can be integrated with the self-training concept by generating the pseudo-labels from the teacher network and training the student network with these pseudo-labels. In order to obtain pseudo-labels as accurately as possible, we do not apply augmentation to the input of the student network. The continuous update of the teacher network enables gradually improved pseudo-labels during training. Xie et al. (Xie et al., 2020) showed that deliberately adding noise to the student model leads to a better teacher model. Following the same principle, we applied an input noise using photometric augmentation and MOCM.

For the segmentation task, the teacher network \mathcal{T} takes an image $x_T^i \in X_T \subset \mathbb{R}^{H \times W \times 3}$ and generate a class probability distribution $p_T \in P_T \subset \mathbb{R}^{H \times W \times C}$ for each pixel, where H , W , and C correspond to the image height, the image width and the number of classes, respectively. The pseudo-label map $\tilde{y} \in \mathbb{R}^{H \times W \times C}$ is a one-hot vector for each pixel, where the channel corresponding to the maximum prediction confidence is one and the others are zero.

The pixel-wise cross-entropy loss is a widely used criterion in semantic segmentation tasks. We adapted the cross-entropy loss to train the student network. Different from the existing methods, all pseudo-labels are taken into account to train the student network. However, the gradients computed by pseudo-labels are scaled based on the label’s reliability. We multiply pixel-wise loss values with the gradient scaling factor using Hadamard multiplication to scale the gradients. The gradient scaling factor $w^{(w,h)}$ is a real-valued map taking values between 0 and 1, and it is calculated based on the reliability metric, explained in section 3.3 in detail.

3.3. Reliability metric learning

The gradient scaling factor (w) plays an important role in the training of the student model. It has a strong effect on the parameters of the student model since it manipulates the gradients. In addition to that, the student model parameters directly affect the teacher model’s performance and consequently the quality of the pseudo-labels. Therefore, It is essential to estimate a good reliability metric in the target domain to calculate

the scaling factor. To this end, we proposed a novel reliability metric predicted by the metric network \mathcal{M} . The metric network utilizes the same architecture with the classifier C of the segmentation network. It takes the features of the feature extractor network \mathcal{F} of the teacher network \mathcal{T} , and predicts a pixel-wise metric feature $f \in \mathbb{R}^{H \times W \times N_f}$, corresponding one metric feature for each input image pixel. The metric network \mathcal{M} learns a transformation from the segmentation feature space to the metric feature space, where the features of the pixels belonging to the same class are pulled together, and those of the pixels belonging to different classes are pushed away.

The metric learning methods commonly use two different relations to train the model, namely pair-based and proxy-based relations. The pair-based methods use data-to-data similarity to train the network, whereas the proxy-based network uses proxy-to-data similarity. We exploit a proxy based relation in our study. The proxy feature $f_p \in \mathbb{R}^{N_f}$ is a vector that represents the distribution of a class of data points. We assign a different proxy feature to each segmentation class since we want to estimate how much the data point is associated with the predicted class. The proxy features are defined as a trainable parameter just as the metric learning network parameters, and it is trained concurrently with the metric network parameters.

Metric learning is a supervised learning method that requires class labels to be trained. Since the proxy-based method is known to be trained with a small number of samples (Movshovitz-Attias et al., 2017; Teh et al., 2020), we use a small subset of the predictions of the teacher network with high confidence values to train the metric network. This subset is called the metric pseudo-labels, and they are selected with class balanced thresholding strategy.

$$\tilde{y}_M^{h,w,c} = \begin{cases} 1 & p_T^{h,w,c} = \max(p_T^{h,w}) > \tau_c \\ 0 & elsewhere \end{cases} . \quad (1)$$

Threshold values (τ) are varied for each class. Class-balanced thresholding strategy (Zou et al., 2018) selects a certain percentile (q_M) of the prediction confidences. We choose a low percentile value to obtain highly confident predictions.

Threshold values are calculated in training time with the moving average of the percentile of the prediction of the current frame.

One successful approach in proxy-based metric learning is to use neighborhood component analysis (NCA) in training, where the samples are compared against proxies. The proxy features and the metric network parameters are updated concurrently to attract the feature of a sample to the corresponding proxy feature and repel from the other proxy features. We apply a similar approach to train the metric network and proxy features. Teh et al. (Teh et al., 2020) show that using small temperature T values refine decision boundaries and help classify samples better. Motivated by these, we utilize NCA with temperature scaling. We select an equal number of samples in each class in $\hat{y}_M^{h,w,c}$ to ensure balanced training. The metric network is optimized the following loss function:

$$\mathcal{L}_M = \sum_{h,w} \left[-\log \left(\frac{\exp(-d(f^{h,w}, f_p) * \frac{1}{T})}{\sum_c \exp(-d(f^{h,w}, f_{p_c}) * \frac{1}{T})} \right) \right], \quad (2)$$

where T is a temperature and $d(x, y)$ is a normalized squared L2-Norm:

$$d(x, y) = \sum_i \left(\frac{x_i}{\|x\|} - \frac{y_i}{\|y\|} \right)^2 \quad (3)$$

The same distance function is used in both training the metric network and calculating the reliability score. The smaller the distance gets, the more similar to the corresponding class it becomes. In order to calculate the similarity, we first feed the features of the feature extractor network of the teacher model to the metric network. The metric network outputs a metric feature for each pixel of the input image of the teacher network. Then we generate the similarity map by calculating the distance between the metric features and the proxy feature of the class predicted by the teacher network. We use a reverse sigmoid function to transform similarity to the reliability, where α is sharpness constant, and β is offset of the sigmoid function:

$$w^{(h,w)} = \frac{1}{1 + e^{-\alpha * (\beta - d(f^{h,w}, \hat{f}_p))}} \quad (4)$$

3.4. Metric-based online ClassMix

The noise injection to the input of the student model leads to a better generalization for both the student and teacher model (Xie et al., 2020). Data augmentation with photometric noise is a common approach in computer vision applications. Another effective augmentation technique for classification and semantic segmentation is the mixing method. The mixing methods combine pixels from two training images to create a highly perturbed sample. ClassMix algorithm (Olsson et al., 2021) is a mixing data augmentation method that cuts half of the classes in the predicted image and pastes on the other image.

In the context of source-free domain adaptation, the unavailability of the source dataset restricts the ability to mix target data with the source data. Additionally, the absence of labels in the target dataset prevents the extraction of class patches from the target images based on groundtruth information. To address this challenge, we propose a method called Metric-based Online ClassMix (MOCM). This method effectively stores reliable patches during the training phase using metric distance and subsequently incorporates these patches into the input data.

We maintain separate patch buffers for each class. These buffers have a fixed size and operate on a first-in-first-out scheme, effectively reducing memory requirements while ensuring that the most up-to-date patches are stored. To select which patches to store, we utilize the distance between the metric feature predicted by the metric network and the proxy features. If the average distance between the metric features and the corresponding class proxy (f_p^c) of a patch falls below a predefined threshold (τ_{MOCM}), the patch is added to the buffer of class c . Since the mixing operation occurs in both image and label space, we store the image, pseudo-label, and reliability map patch tuple in the buffer.

To utilize the stored patches, we first apply a photometric noise to the input image, then apply the proposed MOCM method. We sample one patch from each N_{MOCM} classes randomly and paste them onto the image (x_{CM}), pseudo-label (\tilde{y}_{CM}), and reliability map (w_{MOCM}). The training of the student network is performed by the stochastic gradient descent in

Table 1. Comparison with state-of-the-art on GTAV-to-CityScapes in terms of per-class IoUs and mIoU (%). SF represents if the method is in the source-free setting.

| Method | Network | SF | Road | Sidewalk | Building | Wall | Fence | Pole | Light | Sign | Veg. | Terrain | Sky | Person | Rider | Car | Truck | Bus | Train | Mbike | Bicycle | mIoU | |
|--|-----------|-------------|-------------|-------------|-------------|-------------|-------------|-------------|-------------|-------------|-------------|-------------|-------------|-------------|-------------|-------------|-------------|-------------|-------------|-------------|-------------|-------------|------|
| | | | | | | | | | | | | | | | | | | | | | | | |
| AdvEnt (Vu et al., 2019) | DeepLabV2 | ✗ | 89.4 | 33.1 | 81.0 | 26.6 | 26.8 | 27.2 | 33.5 | 24.7 | 83.9 | 36.7 | 78.8 | 58.7 | 30.5 | 84.8 | 38.5 | 44.5 | 1.7 | 31.6 | 32.4 | 45.5 | |
| Intra-domain (Pan et al., 2020) | | ✗ | 90.6 | 37.1 | 82.6 | 30.1 | 19.1 | 29.5 | 32.4 | 20.6 | 85.7 | 40.5 | 79.7 | 58.7 | 31.1 | 86.3 | 31.5 | 48.3 | 0.0 | 30.2 | 35.8 | 45.8 | |
| MaxSquare (Chen et al., 2019a) | | ✗ | 89.4 | 43.0 | 82.1 | 30.5 | 21.3 | 30.3 | 34.7 | 24.0 | 85.3 | 39.4 | 78.2 | <u>63.0</u> | <u>22.9</u> | 84.6 | 36.4 | 43.0 | 5.5 | 34.7 | 33.5 | 46.4 | |
| LSE + FL (Subhani and Ali, 2020) | | ✗ | 90.2 | 40.0 | 83.5 | 31.9 | 26.4 | 32.6 | 38.7 | 37.5 | 81.0 | 34.2 | 84.6 | 61.6 | <u>33.4</u> | 82.5 | 32.8 | 45.9 | 6.7 | 29.1 | 30.6 | 47.5 | |
| BDL (Li et al., 2019) | | ✗ | 91.0 | 44.7 | 84.2 | 34.6 | 27.6 | 30.2 | 36.0 | 36.0 | 85.0 | 43.6 | 83.0 | 58.6 | 31.6 | 83.3 | 35.3 | 49.7 | 3.3 | 28.8 | 35.6 | 48.5 | |
| Stuff and Things (Wang et al., 2020b) | | ✗ | 90.6 | 44.7 | 84.8 | 34.3 | 28.7 | 31.6 | 35.0 | 37.6 | 84.7 | 43.3 | 85.3 | 57.0 | 31.5 | 83.8 | 42.6 | 48.5 | 1.9 | 30.4 | 39.0 | 49.2 | |
| Texture Invariant (Kim and Byun, 2020) | | ✗ | ✗ | 92.9 | 55.0 | 85.3 | 34.2 | 31.1 | 34.9 | 40.7 | 34.0 | 85.2 | 40.1 | 87.1 | 61.0 | 31.1 | 82.5 | 32.3 | 42.9 | 0.3 | 36.4 | 46.1 | 50.2 |
| FDA (Yang and Soatto, 2020) | | ✗ | 92.5 | 53.3 | 82.4 | 26.5 | 27.6 | <u>36.4</u> | 40.6 | 38.9 | 82.3 | 39.8 | 78.0 | 62.6 | 34.4 | 84.9 | 34.1 | 53.1 | 16.9 | 27.7 | 46.4 | 50.4 | |
| DMLC (Guo et al., 2021) | | ✗ | <u>92.8</u> | 58.1 | 86.2 | 39.7 | <u>33.1</u> | 36.3 | 42.0 | 38.6 | 85.5 | 37.8 | 87.6 | 62.8 | 31.7 | 84.8 | 35.7 | 50.3 | 2.0 | 36.8 | 48.0 | 52.1 | |
| URMA (Fleuret et al., 2021) | | ✓ | <u>92.3</u> | <u>55.2</u> | 81.6 | 30.8 | 18.8 | 37.1 | 17.7 | 12.1 | 84.2 | 35.9 | 83.8 | 57.7 | 24.1 | 81.7 | 27.5 | 44.3 | <u>6.9</u> | 24.1 | 40.4 | 45.1 | |
| LD (You et al., 2021) | | ✓ | 91.6 | 53.2 | 80.6 | 36.6 | 14.2 | 26.4 | 31.6 | 22.7 | 83.1 | 42.1 | 79.3 | 57.3 | 26.6 | 82.1 | 41.0 | 50.1 | 0.3 | 25.9 | 19.5 | 45.5 | |
| DT+AC (Yang et al., 2022) | | ✓ | 78.0 | 29.5 | 83.0 | 29.3 | 21.0 | 31.8 | 38.1 | 33.1 | 83.8 | 39.2 | 80.8 | 61.0 | 30.0 | 83.9 | 26.1 | 40.4 | 1.9 | 34.2 | 43.7 | 45.7 | |
| SRDA (Bateson et al., 2020) | | ✓ | 90.5 | 47.1 | 82.8 | 32.8 | 28.0 | 29.9 | 35.9 | 34.8 | 83.3 | 39.7 | 76.1 | 57.3 | 23.6 | 79.5 | 30.7 | 40.2 | 0.0 | 26.6 | 30.9 | 45.8 | |
| HCL (Huang et al., 2021) | | ✓ | 92.0 | 55.0 | 80.4 | 33.5 | 24.6 | 37.1 | 35.1 | 28.8 | 83.0 | 37.6 | 82.3 | 59.4 | 27.6 | 83.6 | 32.3 | 36.6 | 14.1 | 28.7 | 43.0 | 48.1 | |
| STvM (w/o MST) | DeepLabV2 | ✓ | 91.4 | 52.9 | <u>87.3</u> | <u>41.5</u> | 33.3 | 35.9 | 40.8 | <u>48.5</u> | <u>87.3</u> | <u>49.2</u> | <u>87.4</u> | 62.2 | 9.3 | 87.1 | <u>45.5</u> | <u>58.7</u> | 0.0 | <u>47.4</u> | <u>59.8</u> | <u>54.0</u> | |
| STvM (w/ MST) | | ✓ | 92.1 | 55.1 | 87.6 | 45.5 | 33.3 | 36.1 | <u>41.8</u> | 48.6 | 87.9 | 51.1 | 87.6 | 63.2 | 8.6 | <u>87.0</u> | 47.8 | 59.8 | 0.0 | 50.1 | 60.4 | 54.9 | |
| MinEnt (Vu et al., 2019) | DeepLabV3 | ✗ | 80.2 | 31.9 | 81.4 | 25.1 | 20.8 | 24.6 | 30.2 | 17.5 | 83.2 | 18.0 | 76.2 | 55.2 | 24.6 | 75.5 | 33.2 | 31.2 | 4.4 | 27.4 | 22.9 | 40.2 | |
| AdaptSegNet (Tsai et al., 2018) | | ✗ | 81.6 | 26.6 | 79.5 | 20.7 | 20.5 | 23.7 | 29.9 | 22.6 | 81.6 | 26.7 | 81.2 | 52.4 | 20.2 | 79.1 | 36.0 | 28.8 | 7.5 | 24.7 | 26.2 | 40.5 | |
| CBST (Zou et al., 2018) | | ✗ | 84.8 | 41.5 | 80.4 | 19.5 | 22.4 | 24.7 | 30.2 | 20.4 | 83.5 | 29.6 | 82.3 | 54.7 | 25.3 | 79.2 | 34.5 | 32.3 | <u>6.8</u> | <u>29.0</u> | 34.9 | 42.9 | |
| MaxSquare (Chen et al., 2019a) | | ✗ | 85.8 | 33.6 | 82.4 | 25.3 | 25.0 | 26.5 | 33.3 | 18.7 | 83.2 | 32.9 | 79.8 | 57.8 | 22.2 | 81.0 | 32.1 | 32.6 | 5.2 | 29.8 | <u>32.4</u> | 43.1 | |
| SFDA (Liu et al., 2021b) | | ✓ | 84.2 | 39.2 | 82.7 | 27.5 | 22.1 | 25.9 | 31.1 | 21.9 | 82.4 | 30.5 | 85.3 | 58.7 | 22.1 | 80.0 | 33.1 | 31.5 | 3.6 | 27.8 | 30.6 | 43.2 | |
| STvM (w/o MST) | | ✓ | <u>90.3</u> | <u>50.2</u> | <u>87.4</u> | <u>37.9</u> | 33.0 | <u>35.8</u> | <u>45.2</u> | <u>48.5</u> | <u>85.7</u> | 44.1 | <u>86.1</u> | <u>62.4</u> | <u>29.8</u> | <u>84.3</u> | 30.2 | <u>50.0</u> | 0.6 | 7.4 | 0.0 | <u>47.8</u> | |
| STvM (w/ MST) | ✓ | 90.8 | 50.7 | 87.7 | 40.9 | <u>32.0</u> | 36.1 | 47.2 | 48.6 | 85.9 | <u>43.3</u> | 87.0 | 62.9 | 31.5 | 85.2 | <u>34.6</u> | 54.0 | 0.6 | 7.8 | 0.0 | 48.8 | | |

order to minimize the following loss function:

$$\mathcal{L} = \frac{1}{H \times W} \sum \left[\left(- \sum_c \tilde{y}_{MOCM}^{h,w,c} \times \log(T(x_{MOCM})^{h,w,c}) \right) \circ w_{MOCM}^{h,w} \right]. \quad (5)$$

4. Experiments

4.1. Datasets

We demonstrate the performance of STvM on three different source-to-target adaptation scenarios which are GTA5-to-Cityscapes, Synthia-to-Cityscapes, and Cityscapes-to-NTHU Cross-City.

The Cityscapes (Cordts et al., 2016) dataset consists of 5000 real-world street-view images captured in 50 different cities. The images have high-quality pixel-level annotations with a resolution of 2048 x 1024. They are annotated with 19 semantic labels for semantic segmentation. The Cityscapes is split into training, validation, and test sets containing 2975, 500, and

1525 images, respectively. The methods are evaluated on the validation set following the standard setting used in the previous domain adaptation studies. The GTA5 (Richter et al., 2016) is a synthetic dataset where images and labels are automatically grabbed from Grand Theft Auto V video game. It consists of 24,966 synthetic images with the size of 1914 x 1052. They have pixel-level annotations of 33 categories. The 19 classes compatible with the Cityscapes are used in the experiments. The Synthia¹ (Ros et al., 2016) is also a synthetic dataset. It is composed of urban scene images with pixel-level annotations. The commonly used SYNTHIA-RAND-CITYSCAPES subset contains 9,400 images with a resolution of 1280 x 760. The dataset has 16 shared categories with the Cityscapes dataset. Cross-City (Chen et al., 2017c) is a real-world dataset. The images are recorded in four cities, which are Rome, Rio, Taipei, and Tokyo. The dataset has 3200 unlabeled images as a training set and 100 labeled images for the test set with the size of 2048

¹This dataset is subject to the CC-BY-NC-SA 3.0

Table 2. Comparison with state-of-the-art on SYNTHIA-to-CityScapes in terms of per-class IoUs and mIoU (%). The mIoU* column denotes the mean IoU over 13 categories excluding those marked by *, SF represents if the method is in the source-free setting.

| Method | Network | SF | Road | Sidewalk | Building | Wall* | Fence* | Pole* | Light | Sign | Veg. | Sky | Person | Rider | Car | Bus | Mbike | Bicycle | mIoU | mIoU* |
|--|-----------|------|-------------|-------------|-------------|-------------|-------------|-------------|-------------|-------------|-------------|-------------|-------------|-------------|-------------|-------------|-------------|-------------|-------------|-------------|
| AdvEnt (Vu et al., 2019) | DeepLabV2 | ✗ | 85.6 | 42.2 | 79.7 | 8.7 | 0.4 | 25.9 | 5.4 | 8.1 | 80.4 | 84.1 | 57.9 | 23.8 | 73.3 | 36.4 | 14.2 | 33.0 | 41.2 | 48.0 |
| MaxSquare (Chen et al., 2019a) | | ✗ | 82.9 | 40.7 | 80.3 | <u>10.2</u> | 0.8 | 25.8 | 12.8 | 18.2 | 82.5 | 82.2 | 53.1 | 18.0 | 79.0 | 31.4 | 10.4 | 35.6 | 41.5 | 48.2 |
| Intra-domain (Pan et al., 2020) | | ✗ | 84.3 | 37.7 | 79.5 | 5.3 | 0.4 | 24.9 | 9.2 | 8.4 | 80.0 | 84.1 | 57.2 | 23.0 | 78.0 | 38.1 | 20.3 | 36.5 | 41.7 | 48.9 |
| Texture Invariant (Kim and Byun, 2020) | | ✗ | 92.6 | 53.2 | 79.2 | - | - | - | 1.6 | 7.5 | 78.6 | 84.4 | 52.6 | 20.0 | 82.1 | 34.8 | 14.6 | 39.4 | - | 49.3 |
| LSE + FL (Subhani and Ali, 2020) | | ✗ | 82.9 | 43.1 | 78.1 | 9.3 | 0.6 | 28.2 | 9.1 | 14.4 | 77.0 | 83.5 | 58.1 | 25.9 | 71.9 | 38.0 | <u>29.4</u> | 31.2 | 42.5 | 49.4 |
| BDL (Li et al., 2019) | | ✗ | <u>86.0</u> | 46.7 | 80.3 | - | - | - | 14.1 | 11.6 | 79.2 | 81.3 | 54.1 | 27.9 | 73.7 | 42.2 | 25.7 | 45.3 | - | 51.4 |
| Stuff and Things (Wang et al., 2020b) | | ✗ | 83.0 | 44.0 | 80.3 | - | - | - | 17.1 | 15.8 | 80.5 | 81.8 | 59.9 | 33.1 | 70.2 | 37.3 | 28.5 | 45.8 | - | 52.1 |
| FDA (Yang and Soatto, 2020) | | ✗ | 79.3 | 35.0 | 73.2 | - | - | - | 19.9 | 24.0 | 61.7 | 82.6 | 61.4 | <u>31.1</u> | 83.9 | 40.8 | 38.4 | 51.1 | - | 52.5 |
| DMLC (Guo et al., 2021) | | ✗ | 92.6 | <u>52.7</u> | 81.3 | 8.9 | 2.4 | 28.1 | 13.0 | 7.3 | 83.5 | 85.0 | <u>60.1</u> | 19.7 | 84.8 | 37.2 | 21.5 | 43.9 | 45.1 | 52.5 |
| URMA (Fleuret et al., 2021) | | ✓ | 59.3 | 24.6 | 77.0 | 14.0 | <u>1.8</u> | 31.5 | 18.3 | 32.0 | 83.1 | 80.4 | 46.3 | 17.8 | 76.7 | 17.0 | 18.5 | 34.6 | 39.6 | 45.0 |
| DT+AC (Yang et al., 2022) | | ✓ | 77.5 | 37.4 | 80.5 | 13.5 | 1.7 | 30.5 | 24.8 | 19.7 | 79.1 | 83.0 | 49.1 | 20.8 | 76.2 | 12.1 | 16.5 | 46.1 | 41.8 | 47.9 |
| LD (You et al., 2021) | | ✓ | 77.1 | 33.4 | 79.4 | 5.8 | 0.5 | 23.7 | 5.2 | 13.0 | 81.8 | 78.3 | 56.1 | 21.6 | 80.3 | 49.6 | 28.0 | 48.1 | 42.6 | 50.1 |
| HCL (Huang et al., 2021) | | ✓ | 80.9 | 34.9 | 76.7 | 6.6 | 0.2 | <u>36.1</u> | 20.1 | 28.2 | 79.1 | 83.1 | 55.6 | 25.6 | 78.8 | 32.7 | 24.1 | 32.7 | 43.5 | 50.2 |
| STvM (w/o MST) | | ✓ | 71.7 | 31.0 | <u>83.7</u> | 0.2 | 0.1 | 35.8 | <u>34.7</u> | <u>37.9</u> | 84.8 | <u>87.5</u> | 53.6 | 23.0 | <u>85.8</u> | 46.7 | 26.9 | <u>52.6</u> | <u>47.2</u> | <u>55.4</u> |
| STvM (w/ MST) | ✓ | 71.6 | 31.1 | 84.2 | 0.0 | 0.0 | 36.7 | 36.0 | 38.4 | 85.4 | 87.8 | 55.4 | 23.5 | 85.9 | 47.8 | 29.1 | 53.6 | 47.9 | 56.1 | |
| MinEnt (Vu et al., 2019) | DeepLabV3 | ✗ | 78.2 | 39.6 | 81.9 | 4.3 | 0.2 | 26.2 | 2.2 | 4.1 | 81.1 | 87.7 | 37.7 | 7.2 | 75.8 | 24.9 | 4.6 | 25.1 | 36.3 | 42.3 |
| AdaptSegNet (Tsai et al., 2018) | | ✗ | 79.7 | 38.6 | 79.3 | 5.6 | 0.8 | 25.4 | 3.6 | 5.5 | 80.0 | 85.4 | 40.8 | 11.7 | 79.8 | 21.4 | 5.2 | 30.5 | 37.1 | 43.2 |
| CBST (Zou et al., 2018) | | ✗ | <u>81.4</u> | <u>44.2</u> | 80.4 | 7.9 | 0.7 | 25.6 | 5.2 | 12.4 | 81.4 | <u>89.5</u> | 39.7 | 10.6 | <u>82.1</u> | 21.9 | 6.3 | 32.9 | 38.9 | 45.2 |
| MaxSquare (Chen et al., 2019a) | | ✗ | 81.0 | 39.8 | 82.6 | 8.7 | 0.5 | 23.2 | 6.6 | 12.4 | <u>85.3</u> | 90.1 | 39.9 | 8.4 | 84.7 | 19.4 | 10.2 | 33.4 | 39.1 | 45.7 |
| SFDA (Liu et al., 2021b) | | ✓ | 81.9 | 44.9 | 81.7 | 4.0 | 0.5 | 26.2 | 3.3 | 10.7 | 86.3 | 89.4 | 37.9 | 13.4 | 80.6 | 25.6 | 9.6 | 31.3 | 39.2 | 45.9 |
| STvM (w/o MST) | | ✓ | 49.3 | 20.7 | <u>84.2</u> | <u>14.0</u> | <u>1.2</u> | <u>33.1</u> | <u>42.4</u> | <u>45.9</u> | 82.9 | 82.8 | <u>50.4</u> | <u>22.1</u> | 81.1 | <u>38.4</u> | <u>21.2</u> | <u>46.5</u> | <u>44.8</u> | <u>51.4</u> |
| STvM (w/ MST) | ✓ | 45.9 | 19.8 | 84.5 | 15.3 | 1.3 | 33.7 | 44.6 | 46.5 | 83.3 | 84.0 | 51.3 | 23.1 | 80.9 | 40.7 | 24.8 | 47.2 | 45.4 | 52.1 | |

x 1024. Cross-City has 13 shared classes with the Cityscapes dataset.

4.2. Implementation details

To ensure a fair comparison with previous unsupervised source-free domain adaptation methods for semantic segmentation, we employ two different segmentation networks. The first network is DeepLabV2 (Chen et al., 2017a) with the ResNet-101 backbone, and the second network is DeepLabV3 (Chen et al., 2017b) with the ResNet-50 backbone. Both the teacher (\mathcal{T}) and the student (\mathcal{S}) networks adopt the same architecture. ResNet-101 and ResNet-50 are utilized as feature extractors, while the ASPP module of the DeepLabV2 or DeepLabV3 architecture is employed for the classifier (\mathcal{C}) and metric (\mathcal{M}) networks, depending on the chosen architecture.

We perform the experiments on a single NVIDIA RTX 2080 Ti GPU using the PyTorch framework (Paszke et al., 2017). We use the same parameters in the training of both DeepLabV2 and DeepLabV3. We resize the input image to 1024×512 and cropped 512×512 patch randomly in our experiments. The

batch size is set to 2.

Both the student and the teacher network is initialized with the source model which is trained in the source domain. The student network (\mathcal{S}) is trained with the Stochastic Gradient Descent (SGD) (Bottou, 2010) optimizer with Nesterov acceleration. The initial learning rate is set to 2.5×10^{-4} and 2.5×10^{-3} for the feature extractor (\mathcal{F}) and the classifier (\mathcal{C}), respectively. The momentum is set to 0.9, and the weight decay is set to 5.0×10^{-4} . The teacher network is updated once in 100 iterations with the parameters of the student network, setting the smoothing factor as 1.0×10^{-3} . The Adam (Kingma and Ba, 2015) optimizer is utilized for training the metric network (\mathcal{M}) with the initial learning rate of 3.0×10^{-4} . The learning rates of both optimizers are scheduled with polynomial weight decay with the power of 0.9. All the networks are trained concurrently, enabling end-to-end training.

As for the hyper-parameters, metric feature size N_f , metric temperature T , metric pseudo-label threshold percentile q_m and the patch buffer size are set to 128, 0.25, 0.2 and 50, respectively. The metric distance to reliability transformation param-

Table 3. Comparison with state-of-the-art on CityScapes-to-NTHU in terms of mIoU (%). DL V2 and DL V3 represents DeepLabV2 with ResNet-101 backbone and DeepLabV3 with ResNet-50 backbone, respectively.

| Method | Network | Rome | Rio | Tokyo | Taipei | Mean |
|-----------------------------|---------|-------------|-------------|-------------|-------------|-------------|
| URMA (Fleuret et al., 2021) | DL V2 | <u>53.8</u> | 53.5 | 49.8 | 50.1 | 51.8 |
| STvM (w/o MST) | | 53.1 | <u>54.5</u> | <u>51.6</u> | <u>51.4</u> | <u>52.6</u> |
| STvM (w/ MST) | | 54.2 | 56.8 | 52.7 | 53.4 | 54.3 |
| SFDA (Liu et al., 2021b) | DL V3 | 48.3 | 49.0 | 46.4 | 47.2 | 47.7 |
| STvM (w/o MST) | | <u>50.8</u> | <u>51.0</u> | <u>46.1</u> | 45.0 | <u>48.2</u> |
| STvM (w/ MST) | | 51.2 | 52.6 | 46.4 | <u>46.0</u> | 49.0 |

eters α and β are set to 2 and 0.6. The metric distance threshold τ_{MOCM} is set to 0.8.

4.3. Results

We evaluated our proposed method STvM on two challenging synthetic-to-real and one cross-city domain adaptation scenarios, namely GTA5-to-CityScapes, SYNTHIA-to-CityScapes, and CityScapes-to-Cross-City settings. We compared our method with the state-of-the-art methods, containing both classical and source-free methods. The results, obtained with two network architectures, are given in Table 1, 2, and 3. MST corresponds to multi-scale testing.

Classical domain adaptation methods, utilizing the labeled source-domain dataset alongside the unlabeled target dataset, gain the advantage of better convergence than source-free domain adaptation methods. Therefore, they usually perform better than source-free settings.

STvM is a source-free domain adaptation method. The experimental results show that our method outperforms the state-of-the-art methods in the same class by a large margin. Specifically, It improves the performance of SRDA by 20% on the GTA5-to-CityScapes dataset with DeepLabV2, SFDA by %14 on SYNTHIA-to-CityScapes dataset with DeepLabV3, and SFDA by 13% on the GTA5-to-CityScapes dataset with DeepLabV3. We observed that metric learning is a powerful tool for discriminating confusing classes such as building/wall and light/sign. In addition, STvM shows better or comparable

performance with the classical domain adaptation methods.

4.3.1. Ablation study

In order to analyze the effect of each component on the performance, we present the results of the ablation study in Table 4. We named the methods as *Source*, *ST*, *ST_{Aug}*, *ST_{MT}*, *STvM_{Raw}*, and *STvM*. *Source* is a model trained in source-domain without any domain adaptation method is applied. *ST* model represents a network trained with the self-training (ST) method using all pseudo-labels. Conforming the common knowledge, the self-training boosts the performance of the source model by +6.8%. *ST_{Aug}* utilizes both self-training (ST) and photometric augmentation (Aug.) to the input image. Injection of the photometric noise to the self-training provides +2.1% improvement. *ST_{MT}* follows the mean teacher (MT) approach. All predictions of the teacher network are used as pseudo-labels to train the student network. While photometric augmentation is applied to the input of the student, no augmentation is applied to the input of the teacher network. Enabling mean-teacher with self-training by using all the predictions of the teacher model contributes +2.4%. As an extension to the *ST_{MT}*, *STvM_{Raw}* benefits from the gradient scaling (GS). The metric network is used to estimate the reliability of the predictions of the teacher network. The metric network that generates reliability to scale gradients of the predictions improves performance by +1.4% showing the effectiveness of the proposed method. *STvM* also exploits the metric-based online ClassMix (MOCM). Using the metric distance in the generation of the patches improves performance significantly. Generating patches and mixing with the input in training time using the reliability has a strong positive impact on the performance by +4.7%.

4.3.2. Hyper-Parameter analysis

In order to evaluate the influence of the hyper-parameters, we conduct experiments for four different values of all hyper-parameters: MOCM threshold (τ_{MOCM}), MOCM patch per image (N_{MOCM}), metric feature size (N_f), metric proxy temperature (T), metric pseudo-label quantile (q_M), reverse sigmoid

Table 4. Ablation Study on GTAV-to-CityScapes

| Name | ST | Aug. | MT | MGS | MOCM | mIoU | Δ |
|---------------------------|----|------|----|-----|------|-------------|-------------|
| <i>Source</i> | - | - | - | - | - | 36.6 | - |
| <i>ST</i> | ✓ | - | - | - | - | 43.4 | +6.8 |
| <i>ST_{Aug}</i> | ✓ | ✓ | - | - | - | 45.5 | +2.1 |
| <i>ST_{MT}</i> | ✓ | ✓ | ✓ | - | - | 47.9 | +2.4 |
| <i>STvM_{Raw}</i> | ✓ | ✓ | ✓ | ✓ | - | 49.3 | +1.4 |
| <i>STvM</i> | ✓ | ✓ | ✓ | ✓ | ✓ | 54.0 | +4.7 |

alpha (α), reverse sigmoid beta (β). The experimental results are given in Table 5. The parameter stated in the name column is modified in the experiments. The default values are kept for the rest. We observed that no parameter has a noteworthy impact on the performance except large α and small N_{MOCM} values. Assigning large α leads to a sharp decrease in the reliability of the sample that limits the contribution of the samples that are far away to the corresponding proxy. This is a desirable situation for the perfectly trained metric network. However, the metric network is trained with highly-confident predictions of the teacher network. Therefore, the metric network is overconfident for the easy samples. If large α is selected, the student network is biased towards easy samples. That decreases diversity and has a negative impact on performance. Using a small N_{MOCM} value decreases the complexity of the augmentation, limiting the contribution of the proposed metric-based online ClassMix method.

Table 5. HyperParameter Analysis on GTAV-to-CityScapes

| Name | Parameter Value / Performance | | | |
|---------------|-------------------------------|-------------|------------|------------|
| τ_{MOCM} | 0.4 / 52.9 | 0.6 / 53.07 | 0.8 / 54.0 | 1.0 / 53.0 |
| N_{MOCM} | 2 / 51.1 | 5 / 52.4 | 10 / 54.0 | 15 / 53.5 |
| N_f | 32 / 53.1 | 64 / 53.0 | 128 / 54.0 | 256 / 52.9 |
| T | 0.1 / 53.8 | 0.25 / 54.0 | 0.5 / 52.9 | 1.0 / 52.3 |
| q_M | 0.1 / 52.6 | 0.2 / 54.0 | 0.3 / 53.5 | 0.4 / 53.3 |
| α | 1 / 53.1 | 2 / 54.0 | 4 / 51.3 | 8 / 50.0 |
| β | 0.5 / 53.0 | 0.6 / 54.0 | 0.7 / 53.6 | 0.8 / 53.8 |

4.3.3. Variance analysis

We made a variance analysis for our STvM and compared it to state-of-the-art methods. Following URMA (Fleuret et al., 2021), we conduct five experiments with different random seeds, keeping the hyper-parameters in their default values. The mean and standard deviations obtained for GTA5-to-CityScapes with DeepLabV2 are reported in Table 6. Experiments show that STvM shows robust performance with the lowest standard deviation among the state-of-the-art methods.

Table 6. Variance Analysis on GTAV-to-CityScapes

| Method | Performance Estimate | Min |
|-------------|------------------------------------|--------------|
| AdaptSegnet | 39.68 ± 1.49 | 37.70 |
| ADVENT | 42.56 ± 0.64 | 41.60 |
| CBST | 44.04 ± 0.88 | 42.80 |
| UMRA | 42.44 ± 2.18 | 39.71 |
| STvM | 53.55 ± 0.25 | 53.26 |

4.3.4. Metric network evaluation

The metric network clusters classes in the metric feature space, providing a reliable distance measure. The silhouette score is a widely used metric to calculate the goodness of the clustering method. We utilize the silhouette score to evaluate the performance of the metric network. Specifically, we computed the silhouette score (Rousseeuw, 1987) for each pixel of each image of the validation set. The overall mean and the class-wise mean silhouette scores of all validation set is presented in the Table 7. Note that the clustering performance correlates with the segmentation performance, which indicates the collaboration between the metric network and the segmentation network.

Table 7. Metric Evaluation. The class-wise mean and the overall mean silhouette scores.

| Name | Class Mean | Overall Mean |
|---------------------------|-------------|--------------|
| <i>ST_{MT}</i> | 24.3 | 42.0 |
| <i>STvM_{Raw}</i> | 30.1 | 48.3 |
| <i>STvM</i> | 33.5 | 49.1 |

5. Limitations and Future Work

The metric network is the essential component of the STvM. It directly impacts the performance since both the gradient scaling factor and the patch quality to be used in the MOCM are calculated using the metric distance. Even though we use highly reliable predictions of the teacher network, over-confident false predictions may harm the performance of the metric network. Therefore, better supervision would be beneficial. Recently, self-supervised training techniques have shown promising results. Note that metric learning does not need class labels, but it needs discriminative labels. Therefore, we believe that training the metric network with self-supervised training techniques would help the overall performance.

6. Conclusion

We proposed a self-training via metric learning (STvM) framework utilizing the mean-teacher approach for the source-free domain adaptation method of semantic segmentation. STvM learns a metric feature space directly in the target domain using a proxy-based metric learning technique. In training time, a reliability score is calculated for the teacher’s predictions by using the distance of the metric features to the class-proxy features. The reliability score is used for scaling gradients and generating object patches. The generated patches are used to augment the input of the student network with the proposed Metric-based Online ClassMix (MOCM) method. The experimental results show that utilizing all the predictions is beneficial for self-training of source-free domain adaptation and also gradient scaling is useful to mitigate the negative impact of false positives pseudo-labels. This self-training strategy also facilitates under-confident positive samples to contribute to training. MOCM augmentation technique highly perturbs the input image, facilitating more robust training. STvM significantly outperforms state-of-the-art methods, and it is highly robust the randomness in training.

During the preparation of this work the author(s) used ChatGPT in order to improve language and readability. After using this tool/service, the author(s) reviewed and edited the content

as needed and take(s) full responsibility for the content of the publication.

References

- Araslanov, N., Roth, S., 2021. Self-supervised augmentation consistency for adapting semantic segmentation, in: *Proceedings of the IEEE/CVF Conference on Computer Vision and Pattern Recognition*, pp. 15384–15394.
- Aziere, N., Todorovic, S., 2019. Ensemble deep manifold similarity learning using hard proxies, in: *Proceedings of the IEEE/CVF Conference on Computer Vision and Pattern Recognition*, pp. 7299–7307.
- Bateson, M., Kervadec, H., Dolz, J., Lombaert, H., Ayed, I.B., 2020. Source-relaxed domain adaptation for image segmentation, in: *International Conference on Medical Image Computing and Computer-Assisted Intervention*, Springer. pp. 490–499.
- Berthelot, D., Carlini, N., Goodfellow, I., Papernot, N., Oliver, A., Raffel, C., 2019. Mixmatch: A holistic approach to semi-supervised learning, in: *NeurIPS*.
- Bottou, L., 2010. Large-scale machine learning with stochastic gradient descent, in: *Proceedings of COMPSTAT’2010*. Springer, pp. 177–186.
- Chang, W.L., Wang, H.P., Peng, W.H., Chiu, W.C., 2019. All about structure: Adapting structural information across domains for boosting semantic segmentation, in: *Proceedings of the IEEE Conference on Computer Vision and Pattern Recognition*, pp. 1900–1909.
- Chen, L.C., Papandreou, G., Kokkinos, I., Murphy, K., Yuille, A.L., 2017a. Deeplab: Semantic image segmentation with deep convolutional nets, atrous convolution, and fully connected crfs. *IEEE transactions on pattern analysis and machine intelligence* 40, 834–848.
- Chen, L.C., Papandreou, G., Schroff, F., Adam, H., 2017b. Rethinking atrous convolution for semantic image segmentation. *arXiv preprint arXiv:1706.05587*.
- Chen, M., Xue, H., Cai, D., 2019a. Domain adaptation for semantic segmentation with maximum squares loss, in: *Proceedings of the IEEE International Conference on Computer Vision*, pp. 2090–2099.
- Chen, Y., Li, W., Chen, X., Gool, L.V., 2019b. Learning semantic segmentation from synthetic data: A geometrically guided input-output adaptation approach, in: *Proceedings of the IEEE Conference on Computer Vision and Pattern Recognition*, pp. 1841–1850.
- Chen, Y., Pont-Tuset, J., Montes, A., Van Gool, L., 2018. Blazingly fast video object segmentation with pixel-wise metric learning, in: *Proceedings of the IEEE conference on computer vision and pattern recognition*, pp. 1189–1198.
- Chen, Y.C., Lin, Y.Y., Yang, M.H., Huang, J.B., 2019c. Crdoco: Pixel-level domain transfer with cross-domain consistency, in: *Proceedings of the IEEE Conference on Computer Vision and Pattern Recognition*, pp. 1791–1800.
- Chen, Y.H., Chen, W.Y., Chen, Y.T., Tsai, B.C., Frank Wang, Y.C., Sun, M., 2017c. No more discrimination: Cross city adaptation of road scene seg-

- menters, in: Proceedings of the IEEE International Conference on Computer Vision, pp. 1992–2001.
- Cheng, D., Gong, Y., Zhou, S., Wang, J., Zheng, N., 2016. Person re-identification by multi-channel parts-based cnn with improved triplet loss function, in: Proceedings of the IEEE conference on computer vision and pattern recognition, pp. 1335–1344.
- Choi, J., Kim, T., Kim, C., 2019. Self-ensembling with gan-based data augmentation for domain adaptation in semantic segmentation, in: Proceedings of the IEEE/CVF International Conference on Computer Vision, pp. 6830–6840.
- Cordts, M., Omran, M., Ramos, S., Rehfeld, T., Enzweiler, M., Benenson, R., Franke, U., Roth, S., Schiele, B., 2016. The cityscapes dataset for semantic urban scene understanding, in: Proceedings of the IEEE conference on computer vision and pattern recognition, pp. 3213–3223.
- Du, L., Tan, J., Yang, H., Feng, J., Xue, X., Zheng, Q., Ye, X., Zhang, X., 2019. Ssf-dan: Separated semantic feature based domain adaptation network for semantic segmentation, in: Proceedings of the IEEE International Conference on Computer Vision, pp. 982–991.
- Everingham, M., Van Gool, L., Williams, C.K., Winn, J., Zisserman, A., 2010. The pascal visual object classes (voc) challenge. *International journal of computer vision* 88, 303–338.
- Fan, M., Lai, S., Huang, J., Wei, X., Chai, Z., Luo, J., Wei, X., 2021. Rethinking bisenet for real-time semantic segmentation, in: Proceedings of the IEEE/CVF conference on computer vision and pattern recognition, pp. 9716–9725.
- Fleuret, F., et al., 2021. Uncertainty reduction for model adaptation in semantic segmentation, in: Proceedings of the IEEE/CVF Conference on Computer Vision and Pattern Recognition, pp. 9613–9623.
- French, G., Laine, S., Aila, T., Mackiewicz, M., Finlayson, G., 2020. Semi-supervised semantic segmentation needs strong, varied perturbations. *British Machine Vision Conference*.
- Goodfellow, I., Pouget-Abadie, J., Mirza, M., Xu, B., Warde-Farley, D., Ozair, S., Courville, A., Bengio, Y., 2014. Generative adversarial nets. *Advances in neural information processing systems* 27.
- Guo, X., Yang, C., Li, B., Yuan, Y., 2021. Metacorection: Domain-aware meta loss correction for unsupervised domain adaptation in semantic segmentation, in: Proceedings of the IEEE/CVF Conference on Computer Vision and Pattern Recognition, pp. 3927–3936.
- Hein, M., Andriushchenko, M., Bitterwolf, J., 2019. Why relu networks yield high-confidence predictions far away from the training data and how to mitigate the problem, in: Proceedings of the IEEE/CVF Conference on Computer Vision and Pattern Recognition, pp. 41–50.
- Herath, S., Fernando, B., Abbasnejad, E., Hayat, M., Khadivi, S., Harandi, M., Rezatofghi, H., Haffari, G., 2023. Energy-based self-training and normalization for unsupervised domain adaptation, in: Proceedings of the IEEE/CVF International Conference on Computer Vision, pp. 11653–11662.
- Hershey, J.R., Chen, Z., Le Roux, J., Watanabe, S., 2016. Deep clustering: Discriminative embeddings for segmentation and separation, in: 2016 IEEE International Conference on Acoustics, Speech and Signal Processing (ICASSP), IEEE, pp. 31–35.
- Hong, W., Wang, Z., Yang, M., Yuan, J., 2018. Conditional generative adversarial network for structured domain adaptation, in: Proceedings of the IEEE Conference on Computer Vision and Pattern Recognition, pp. 1335–1344.
- Hongyi Zhang, Moustapha Cisse, Y.N.D., Lopez-Paz, D., 2018. mixup: Beyond empirical risk minimization. *International Conference on Learning Representations* URL: <https://openreview.net/forum?id=r1Ddp1-Rb>.
- Hoyer, L., Dai, D., Wang, H., Van Gool, L., 2023. Mic: Masked image consistency for context-enhanced domain adaptation, in: Proceedings of the IEEE/CVF conference on computer vision and pattern recognition, pp. 11721–11732.
- Huang, J., Feris, R.S., Chen, Q., Yan, S., 2015. Cross-domain image retrieval with a dual attribute-aware ranking network, in: Proceedings of the IEEE international conference on computer vision, pp. 1062–1070.
- Huang, J., Guan, D., Xiao, A., Lu, S., 2021. Model adaptation: Historical contrastive learning for unsupervised domain adaptation without source data. *Advances in Neural Information Processing Systems* 34, 3635–3649.
- Iqbal, J., Ali, M., 2020. Msl: Multi-level self-supervised learning for domain adaptation with spatially independent and semantically consistent labeling, in: Proceedings of the IEEE/CVF Winter Conference on Applications of Computer Vision, pp. 1864–1873.
- Karim, N., Mithun, N.C., Rajvanshi, A., Chiu, H.p., Samarasekera, S., Rahnavard, N., 2023. C-sfda: A curriculum learning aided self-training framework for efficient source free domain adaptation, in: Proceedings of the IEEE/CVF Conference on Computer Vision and Pattern Recognition, pp. 24120–24131.
- Kim, M., Byun, H., 2020. Learning texture invariant representation for domain adaptation of semantic segmentation, in: Proceedings of the IEEE/CVF Conference on Computer Vision and Pattern Recognition, pp. 12975–12984.
- Kim, S., Kim, D., Cho, M., Kwak, S., 2020. Proxy anchor loss for deep metric learning, in: Proceedings of the IEEE/CVF Conference on Computer Vision and Pattern Recognition, pp. 3238–3247.
- Kingma, D.P., Ba, J., 2015. Adam: A method for stochastic optimization, in: Bengio, Y., LeCun, Y. (Eds.), 3rd International Conference on Learning Representations, ICLR 2015, San Diego, CA, USA, May 7-9, 2015, Conference Track Proceedings. URL: <http://arxiv.org/abs/1412.6980>.
- Kundu, J.N., Kulkarni, A., Singh, A., Jampani, V., Babu, R.V., 2021. Generalize then adapt: Source-free domain adaptive semantic segmentation, in: Proceedings of the IEEE/CVF International Conference on Computer Vision, pp. 7046–7056.
- Laradji, I.H., Babanezhad, R., 2020. M-adda: Unsupervised domain adaptation with deep metric learning, in: *Domain Adaptation for Visual Understanding*. Springer, pp. 17–31.
- Li, Y., Yuan, L., Vasconcelos, N., 2019. Bidirectional learning for domain adaptation of semantic segmentation, in: Proceedings of the IEEE Conference on

- Computer Vision and Pattern Recognition, pp. 6936–6945.
- Liu, H., Wang, J., Long, M., 2021a. Cycle self-training for domain adaptation. *Advances in Neural Information Processing Systems* 34, 22968–22981.
- Liu, Y., Zhang, W., Wang, J., 2021b. Source-free domain adaptation for semantic segmentation, in: *Proceedings of the IEEE/CVF Conference on Computer Vision and Pattern Recognition*, pp. 1215–1224.
- Mei, K., Zhu, C., Zou, J., Zhang, S., 2020. Instance adaptive self-training for unsupervised domain adaptation. *Proceedings of the European Conference on Computer Vision*.
- Movshovitz-Attias, Y., Toshev, A., Leung, T.K., Ioffe, S., Singh, S., 2017. No fuss distance metric learning using proxies, in: *Proceedings of the IEEE International Conference on Computer Vision*, pp. 360–368.
- Oh Song, H., Xiang, Y., Jegelka, S., Savarese, S., 2016. Deep metric learning via lifted structured feature embedding, in: *Proceedings of the IEEE conference on computer vision and pattern recognition*, pp. 4004–4012.
- Olsson, V., Tranheden, W., Pinto, J., Svensson, L., 2021. Classmix: Segmentation-based data augmentation for semi-supervised learning, in: *Proceedings of the IEEE/CVF Winter Conference on Applications of Computer Vision*, pp. 1369–1378.
- Pan, F., Shin, I., Rameau, F., Lee, S., Kweon, I.S., 2020. Unsupervised intra-domain adaptation for semantic segmentation through self-supervision, in: *Proceedings of the IEEE/CVF Conference on Computer Vision and Pattern Recognition*, pp. 3764–3773.
- Paszke, A., Gross, S., Chintala, S., Chanan, G., Yang, E., DeVito, Z., Lin, Z., Desmaison, A., Antiga, L., Lerer, A., 2017. Automatic differentiation in pytorch.
- Pinheiro, P.O., 2018. Unsupervised domain adaptation with similarity learning, in: *Proceedings of the IEEE Conference on Computer Vision and Pattern Recognition*, pp. 8004–8013.
- Qian, Q., Shang, L., Sun, B., Hu, J., Li, H., Jin, R., 2019. Softtriple loss: Deep metric learning without triplet sampling, in: *Proceedings of the IEEE/CVF International Conference on Computer Vision*, pp. 6450–6458.
- Richter, S.R., Vineet, V., Roth, S., Koltun, V., 2016. Playing for data: Ground truth from computer games, in: *Leibe, B., Matas, J., Sebe, N., Welling, M. (Eds.), Proceedings of the European Conference on Computer Vision, Springer International Publishing*, pp. 102–118.
- Ros, G., Sellart, L., Materzynska, J., Vazquez, D., Lopez, A.M., 2016. The synthia dataset: A large collection of synthetic images for semantic segmentation of urban scenes, in: *The IEEE Conference on Computer Vision and Pattern Recognition (CVPR)*.
- Rousseeuw, P.J., 1987. Silhouettes: a graphical aid to the interpretation and validation of cluster analysis. *Journal of computational and applied mathematics* 20, 53–65.
- Sankaranarayanan, S., Balaji, Y., Jain, A., Lim, S.N., Chellappa, R., 2018. Learning from synthetic data: Addressing domain shift for semantic segmentation, in: *Proceedings of the IEEE Conference on Computer Vision and Pattern Recognition*, pp. 3752–3761.
- Schroff, F., Kalenichenko, D., Philbin, J., 2015. Facenet: A unified embedding for face recognition and clustering, in: *Proceedings of the IEEE conference on computer vision and pattern recognition*, pp. 815–823.
- Sohn, K., 2016. Improved deep metric learning with multi-class n-pair loss objective, in: *Advances in neural information processing systems*, pp. 1857–1865.
- Subhani, M.N., Ali, M., 2020. Learning from scale-invariant examples for domain adaptation in semantic segmentation. *Proceedings of the European Conference on Computer Vision*.
- Tarvainen, A., Valpola, H., 2017. Mean teachers are better role models: Weight-averaged consistency targets improve semi-supervised deep learning results. *arXiv preprint arXiv:1703.01780*.
- Teh, E.W., DeVries, T., Taylor, G.W., 2020. Proxynca++: Revisiting and revitalizing proxy neighborhood component analysis, in: *Computer Vision—ECCV 2020: 16th European Conference, Glasgow, UK, August 23–28, 2020, Proceedings, Part XXIV* 16, Springer, pp. 448–464.
- Toldo, M., Maracani, A., Michieli, U., Zanuttigh, P., 2020. Unsupervised domain adaptation in semantic segmentation: a review. *Technologies* 8, 35.
- Tranheden, W., Olsson, V., Pinto, J., Svensson, L., 2021. Dacs: Domain adaptation via cross-domain mixed sampling, in: *Proceedings of the IEEE/CVF Winter Conference on Applications of Computer Vision*, pp. 1379–1389.
- Tsai, Y.H., Hung, W.C., Schulter, S., Sohn, K., Yang, M.H., Chandraker, M., 2018. Learning to adapt structured output space for semantic segmentation, in: *Proceedings of the IEEE Conference on Computer Vision and Pattern Recognition*, pp. 7472–7481.
- Vu, T.H., Jain, H., Bucher, M., Cord, M., Pérez, P., 2019. Advent: Adversarial entropy minimization for domain adaptation in semantic segmentation, in: *Proceedings of the IEEE conference on computer vision and pattern recognition*, pp. 2517–2526.
- Wang, J., Sun, K., Cheng, T., Jiang, B., Deng, C., Zhao, Y., Liu, D., Mu, Y., Tan, M., Wang, X., et al., 2020a. Deep high-resolution representation learning for visual recognition. *IEEE transactions on pattern analysis and machine intelligence*.
- Wang, M., Deng, W., 2018. Deep visual domain adaptation: A survey. *Neurocomputing* 312, 135–153.
- Wang, X., Han, X., Huang, W., Dong, D., Scott, M.R., 2019a. Multi-similarity loss with general pair weighting for deep metric learning, in: *Proceedings of the IEEE/CVF Conference on Computer Vision and Pattern Recognition*, pp. 5022–5030.
- Wang, X., Hua, Y., Kodirov, E., Hu, G., Garnier, R., Robertson, N.M., 2019b. Ranked list loss for deep metric learning, in: *Proceedings of the IEEE/CVF Conference on Computer Vision and Pattern Recognition*, pp. 5207–5216.
- Wang, Z., Yu, M., Wei, Y., Feris, R., Xiong, J., Hwu, W.m., Huang, T.S., Shi, H., 2020b. Differential treatment for stuff and things: A simple unsupervised domain adaptation method for semantic segmentation, in: *Proceedings of the IEEE/CVF Conference on Computer Vision and Pattern Recognition*, pp. 12635–12644.
- Xie, Q., Luong, M.T., Hovy, E., Le, Q.V., 2020. Self-training with noisy student improves imagenet classification, in: *Proceedings of the IEEE/CVF Confer-*

- ence on Computer Vision and Pattern Recognition, pp. 10687–10698.
- Xu, H., Yang, M., Deng, L., Qian, Y., Wang, C., 2021. Neutral cross-entropy loss based unsupervised domain adaptation for semantic segmentation. *IEEE Transactions on Image Processing* 30, 4516–4525.
- Xu, J., Xiong, Z., Bhattacharyya, S.P., 2023. Pidnet: A real-time semantic segmentation network inspired by pid controllers, in: *Proceedings of the IEEE/CVF conference on computer vision and pattern recognition*, pp. 19529–19539.
- Yang, C.Y., Kuo, Y.J., Hsu, C.T., 2022. Source free domain adaptation for semantic segmentation via distribution transfer and adaptive class-balanced self-training, in: *2022 IEEE International Conference on Multimedia and Expo (ICME)*, IEEE, pp. 1–6.
- Yang, Y., Soatto, S., 2020. Fda: Fourier domain adaptation for semantic segmentation, in: *Proceedings of the IEEE/CVF Conference on Computer Vision and Pattern Recognition*, pp. 4085–4095.
- You, F., Li, J., Zhu, L., Chen, Z., Huang, Z., 2021. Domain adaptive semantic segmentation without source data, in: *Proceedings of the 29th ACM international conference on multimedia*, pp. 3293–3302.
- Yu, B., Liu, T., Gong, M., Ding, C., Tao, D., 2018. Correcting the triplet selection bias for triplet loss, in: *Proceedings of the European Conference on Computer Vision (ECCV)*, pp. 71–87.
- Yun, S., Han, D., Oh, S.J., Chun, S., Choe, J., Yoo, Y., 2019. Cutmix: Regularization strategy to train strong classifiers with localizable features, in: *Proceedings of the IEEE/CVF International Conference on Computer Vision*, pp. 6023–6032.
- Zhang, Q., Zhang, J., Liu, W., Tao, D., 2019. Category anchor-guided unsupervised domain adaptation for semantic segmentation. *arXiv preprint arXiv:1910.13049*.
- Zheng, Z., Yang, Y., 2021. Rectifying pseudo label learning via uncertainty estimation for domain adaptive semantic segmentation. *International Journal of Computer Vision* 129, 1106–1120.
- Zhong, Z., Lin, Z.Q., Bidart, R., Hu, X., Daya, I.B., Li, Z., Zheng, W.S., Li, J., Wong, A., 2020. Squeeze-and-attention networks for semantic segmentation, in: *Proceedings of the IEEE/CVF Conference on Computer Vision and Pattern Recognition*, pp. 13065–13074.
- Zhou, W., Wang, Y., Chu, J., Yang, J., Bai, X., Xu, Y., 2020. Affinity space adaptation for semantic segmentation across domains. *IEEE Transactions on Image Processing* 30, 2549–2561.
- Zou, Y., Yu, Z., Liu, X., Kumar, B., Wang, J., 2019. Confidence regularized self-training, in: *Proceedings of the IEEE International Conference on Computer Vision*, pp. 5982–5991.
- Zou, Y., Yu, Z., Vijaya Kumar, B., Wang, J., 2018. Unsupervised domain adaptation for semantic segmentation via class-balanced self-training, in: *Proceedings of the European conference on computer vision (ECCV)*, pp. 289–305.